RACSAM
Rev. R. Acad. Cien. Serie A. Mat.
VOL. **96** (3), 2002, pp. 322–341
Matemática Aplicada / Applied Mathematics
Artículo panorámico / Survey

Numerical simulation of internal tides in the Strait of Gibraltar

M. J. Castro, J. M. González-Vida, J. Macías, M. L. Muñoz, C. Parés, J. García-Rodríguez and E. Vázquez-Cendón

Dedicated to the memory of J.-L. Lions

Abstract. A two-layer one-dimensional numerical model developed for the simulation of flows through channels with irregular geometry both in breadth and depth is used for the study of the internal tides taking place at the Strait of Gibraltar. First, model equations and the numerical scheme used are presented. Then model performance is tested comparing the numerical solutions for simplified channel geometries with the analytical approximate stationary solutions provided by *Armi and Farmer*. Maximal exchange solutions for these channel geometries are obtained from lock exchange experiments. Some results for a barotropic periodical forcing as those obtained by *Helfrich* (1995) are also presented. Finally the model is used to simulate the location and evolution of the interface separating the Atlantic from the Mediterranean waters in the Strait of Gibraltar. Real bathymetric data were considered to include in the model the abrupt geometry of this natural strait. Newly, the maximal exchange solution resulting from lock exchange initial conditions is numerically found, and the evolution of the interface along a tidal period is also presented.

Simulación numérica de mareas internas en el Estrecho de Gibraltar

Resumen. Presentamos un modelo numérico unidimensional para flujos bicapa que se ha desarrollado para la simulación de flujos a través de canales con geometría irregular tanto en anchura como en profundidad. Este modelo se utiliza para el estudio y simulación de las mareas internas que tienen lugar en el Estrecho de Gibraltar. En primer lugar presentamos las ecuaciones del modelo y el esquema numérico que se usa para su resolución. A continuación evaluamos el buen hacer del modelo numérico comparando las soluciones suministradas por éste para canales con geometrías simples con las soluciones estacionarias analíticas aproximadas obtenidas por *Armi y Farmer*. Para estos canales de geometría sencilla las soluciones de intercambio máximo se obtienen de la integración del modelo a partir de condiciones iniciales de tipo "lock-exchange". También se presentan resultados análogos a los de *Helfrich* (1995) para un forzamiento barotrópico que varía de forma periódica. Por último llevamos a cabo la simulación de la posición y movimiento de la interfaz que separa las aguas atlánticas de superficie de las aguas mediterráneas que fluyen en profundidad a través del Estrecho de Gibraltar. En esta simulación se han tomado datos batimétricos reales para incluir en el modelo el efecto de la geometría abrupta de este canal natural en la evolución de la interfaz. De nuevo las soluciones de intercambio máximo, ahora para esta geometría realista, se obtienen a partir de un experimento de tipo lock-exchange. Presentaremos resultados mostrando la evolución de la interfaz a lo largo de un ciclo completo de marea

Presentado por Jesús Ildefonso Díaz.
Recibido: 25 de Julio de 2002. *Aceptado*: 9 de Octubre de 2002.
Palabras clave / Keywords: Q-schemes, coupled conservation laws, source terms, 1D shallow water equations, two-layer flows, hyperbolic systems, maximal two-layer exchange flows, Strait of Gibraltar, internal tides.
Mathematics Subject Classifications: 65M99, 76B55, 76B70

Dedicated to the memory of J.-L. Lions

1. Introduction

The Strait of Gibraltar is the sole natural link between the Mediterranean Sea and the Atlantic Ocean. Located at the vicinity of the 36° parallel with its axis slightly turned (about 12°-15°) in its east-west orientation. Its northern and southern boundaries are clearly determined by the Spanish and Moroccan coasts, while the eastern and western boundaries are not so sharply defined. If we consider as western boundary the Trafalgar-Spartel section and as eastern end the Punta Europa-Punta Almina section, the Strait of Gibraltar has a length of about 60 km with a variable width ranging from the 44 km at the west section to the 12-14 km at the so called Tarifa Narrows (the Tarifa-Punta Cires section). Besides the Strait of Gibraltar bathymetry is very irregular with a minimal depth of about 300 meters at the main sill (Camarinal Sill) located between Punta Paloma and Punta Malabata.

The Strait of Gibraltar controls the water mass exchange between the Mediterranean Sea and the Atlantic Ocean. The Mediterranean Sea needs a supply of Atlantic waters to counteract the excess of evaporation in its basin, but this does not imply a one directional flow through this strait. The mean flow is composed of two counter-flowing layers of water: The surface layer of Atlantic less saline water flows eastward toward the most western part of the Mediterranean (the Alboran Sea), while the lower layer of Mediterranean saltier and denser water flows westward toward the Atlantic Ocean. This mean flow is modulated by the predominant semidiurnal tidal flow, by the wind, and by atmospheric pressure variations.

The importance about the understanding of the processes determining the flow through oceanic straits has stimulated the interest in the hydraulics of two-layer exchange flows. The question of what controls or limits the exchange exchange flow is important not only in determining the overall fluid flow, but also in determining what processes influence the flow and how things are likely to change with the greenhouse effect, for example. But, while the study of single-layer hydraulics flows is mature, the development of two-layer theory is still under progress. The key feature of an oceanographic two-layer exchange flow is the production of buoyancy in one or both of the adjacent basins connected by the strait. Thus, for the case of the Strait of Gibraltar, a negative buoyancy is produced in the Mediterranean as the rate of evaporation exceeds that of precipitation and surface runoff combined.

Theoretical investigation on two-layer exchange flows through straits have been carried out before within the framework of the hydraulic theories by [1], [8], and [12]. [1] and [8] have given solutions for the steady and quasi-steady exchange flow through a strait which contains a sill and a lateral contraction. [12] has shown that the exchange flow is a function of two non-dimensional parameters, the dynamic length of the strait and the forcing strength.

This paper is organized as follows: The model and the numerical scheme are briefly described in sections 2 and 3, respectively. Section 4 is devoted to testing the model and presenting some numerical results. First, model performance is tested by comparing the numerical solutions against the approximate analytical solutions provided by *Armi and Farmer* for simplified channel geometries. Then the effects of imposing a periodic barotropic forcing are studied. Finally, the model is used to investigate the two-layer exchange problem in the Strait of Gibraltar: maximal solution and tidally forced effects.

2. Two layer shallow water equations for symmetric channels with arbitrary sections

In order to apply the numerical methods developed by the authors for the two layer shallow water equations for symmetric channels with arbitrary sections, we present a conservative form for these equations (see [6] for more details). The following notation is considered: ρ_i, denotes the densities, supposed to be constant at each layer ($i = 1$ for the upper layer and $i = 2$ for the lower layer), $Q_i(x,t) = v_i(x,t)A_i(x,t)$ is the discharge at each layer, where $A_i(x,t)$ is the cross-section area at location x and time t, and $v_i(x,t)$ is the

velocity. Channel bottom bathymetry at its axis of symmetry is given by $b(x)$. Fluid depth at each layer is denoted by $h_i(x,t),\ i=1,2$ and $\sigma(x,z)$ represents channel breadth, and is related to A_i by the integrals:

$$A_1 = \int_{b+h_2}^{b+h_2+h_1} \sigma(x,z)\,dz, \quad A_2(x,t) = \int_{b}^{b+h_2} \sigma(x,z)\,dz. \tag{1}$$

Finally, $\sigma^b(x) = \sigma(x,b(x))$, $\sigma_3(x,t) = \sigma(x,b(x)+h_2(x,t))$, $\sigma_1(x,t) = \sigma(x,b(x)+h_2(x,t)+h_1(x,t))$ and $\sigma_2(x,t)$ is such that

$$\frac{1}{\sigma_2(x,t)} = \frac{1-r}{\sigma_3(x,t)} + \frac{r}{\sigma_1(x,t)}.$$

The constant r denotes the ratio of densities, $r = \rho_1/\rho_2$. In oceanographical applications, r is always very closed to 1. Using these notations, the system of equations for a 1-d two-layer shallow water flow through a symmetric channel with arbitrary cross-sections can be written as follows:

$$\frac{\partial \mathbf{W}}{\partial t}(x,t) + \frac{\partial \mathbf{F}}{\partial x}(\boldsymbol{\sigma}(x,t), \mathbf{W}(x,t)) = \mathbf{S}(x, \mathbf{W}(x,t)) + \mathbf{B}(\mathbf{W}(x,t))\frac{\partial \mathbf{W}}{\partial x}(x,t), \tag{2}$$

where

$$\mathbf{W}(x,t) = \begin{bmatrix} W_1(x,t) \\ W_2(x,t) \end{bmatrix},\ W_j = \begin{bmatrix} A_j \\ Q_j \end{bmatrix},\ \boldsymbol{\sigma} = \begin{bmatrix} \sigma_1 \\ \sigma_2 \end{bmatrix}\ j=1,2, \tag{3}$$

$$\mathbf{F}(\boldsymbol{\sigma}, \mathbf{W}) = \begin{bmatrix} F(\sigma_1, W_1) \\ F(\sigma_2, W_2) \end{bmatrix},\ F(\sigma_j, W_j) = \begin{bmatrix} Q_j \\ \dfrac{Q_j^2}{A_j} + \dfrac{g}{2\sigma_j}A_j^2 \end{bmatrix},\ j=1,2, \tag{4}$$

$$\mathbf{B}(\mathbf{W}) = \begin{bmatrix} \mathbf{0} & B_1(W_1) \\ B_2(W_2) & \mathbf{0} \end{bmatrix},\ B_j(W_j) = \begin{bmatrix} 0 & 0 \\ -g\dfrac{r^{j-1}}{\sigma_1}A_j & 0 \end{bmatrix},\ j=1,2, \tag{5}$$

and

$$\mathbf{S}(x, \mathbf{W}) = \mathbf{V}(\boldsymbol{\sigma}, \mathbf{W}) + \bar{\mathbf{S}}(x, \mathbf{W}). \tag{6}$$

In this last formula, the source terms have been split into two parts, one corresponding to the derivatives of $\boldsymbol{\sigma}$:

$$\mathbf{V}(\boldsymbol{\sigma}, \mathbf{W}) = \begin{bmatrix} V_1(\sigma_1, W_1) \\ V_2(\sigma_2, W_2) \end{bmatrix},\ V_j(\sigma_j, W_j) = \begin{bmatrix} 0 \\ \frac{g}{2}\left(\frac{1}{\sigma_j}\right)_x A_j^2 \end{bmatrix}, \quad j=1,2 \tag{7}$$

and another corresponding to the breadth and bottom terms:

$$\bar{\mathbf{S}}(x, \mathbf{W}) = \begin{bmatrix} \bar{S}_{1,1}(x, W_1) + \bar{S}_{2,1}(x, W_1) \\ \bar{S}_{1,2}(x, W_2) + \bar{S}_{2,2}(x, W_2) \end{bmatrix},\ \bar{S}_{1,j}(x, W_j) = \begin{bmatrix} 0 \\ -g\dfrac{\sigma^b}{\sigma_j}b' A_j \end{bmatrix}, \tag{8}$$

and

$$\bar{S}_{2,j}(x, W_j) = \begin{bmatrix} 0 \\ g\left[\dfrac{r^{j-1}}{\sigma_1}(I_1 + (j-1)I_2) + \dfrac{(1-r)^{j-1}}{\sigma_{2j-1}}I_2\right] A_j \end{bmatrix},\ j=1,2, \tag{9}$$

where,

$$I_1(x,t) = \int_{b+h_2}^{b+h_2+h_1} \frac{\partial \sigma}{\partial x}(x,z)\,dz, \quad I_2(x,t) = \int_{b}^{b+h_2} \frac{\partial \sigma}{\partial x}(x,z)\,dz. \tag{10}$$

Source terms modelling drag force between the layers, bottom friction or wind effects could also be considered (see [6] for more details).

2.1. Equations in channel with local rectangular cross-section

If local channel sections are supposed to be rectangular, channel breadth only depends on coordinate x, $\sigma(x)$, therefore,

$$S_i(x,t) = h_i(x,t)\,\sigma(x), \quad q_i(x,t) = \frac{Q_i(x,t)}{\sigma(x)}. \tag{11}$$

Considering the relations given above, the previous equations can be written as,

$$\begin{cases} \dfrac{\partial h_1}{\partial t} + \dfrac{\partial q_1}{\partial x} = -\dfrac{\sigma_x}{\sigma} q_1, \\ \dfrac{\partial q_1}{\partial t} + \dfrac{\partial}{\partial x}\left(\dfrac{q_1^2}{h_1} + \dfrac{g}{2}h_1^2\right) = -g h_1 b' - g h_1 \dfrac{\partial h_2}{\partial x} - \dfrac{\sigma_x}{\sigma}\dfrac{q_1^2}{h_1}, \\ \dfrac{\partial h_2}{\partial t} + \dfrac{\partial q_2}{\partial x} = -\dfrac{\sigma_x}{\sigma} q_2, \\ \dfrac{\partial q_2}{\partial t} + \dfrac{\partial}{\partial x}\left(\dfrac{q_2^2}{h_2} + \dfrac{g}{2}h_2^2\right) = -g h_2 b' - \dfrac{\rho_1}{\rho_2} g h_2 \dfrac{\partial h_1}{\partial x} - \dfrac{\sigma_x}{\sigma}\dfrac{q_2^2}{h_2}. \end{cases} \tag{12}$$

3. Numerical scheme

In [5] and [6] some numerical schemes based on Approximate-State Riemann Solvers have been adapted to systems of conservation laws of the type (2). The commonly used technique is to solve a local linear Riemann problem in order to approximate the fluxes at each intercell. In this particular case we use the fact that, for linear problems, the coupling terms with derivatives can be considered as standard flux terms. Nevertheless, another difficulty appears in (2): the specific dependence of the flux on x and t through the breadth σ. In [10] a suitable treatment for this problem is proposed.

The expression of the generalised Q-scheme of Van-Leer for system (2) is as follows:

$$\begin{aligned} \mathbf{W}_i^{n+1} = \mathbf{W}_i^n + & \frac{\Delta t}{\Delta x}\left(\mathbf{F}_{i-1/2} - \mathbf{F}_{i+1/2}\right) \\ & + \frac{\Delta t}{2\Delta x}\left(\widetilde{\mathbf{B}}_{i-1/2}\cdot(\mathbf{W}_i^n - \mathbf{W}_{i-1}^n) + \widetilde{\mathbf{B}}_{i+1/2}\cdot(\mathbf{W}_{i+1}^n - \mathbf{W}_i^n)\right) \\ & + \frac{\Delta t}{2\Delta x}\left(\mathbf{P}_{i-1/2}^{+}\widetilde{\widetilde{\mathbf{S}}}_{i-1/2} + \mathbf{P}_{i+1/2}^{-}\widetilde{\widetilde{\mathbf{S}}}_{i+1/2}\right) \\ & + \frac{\Delta t}{2\Delta x}\left(\widetilde{\mathbf{C}}_{i-1/2} + \widetilde{\mathbf{C}}_{i+1/2}\right), \end{aligned} \tag{13}$$

with

$$\mathbf{F}_{i+1/2} = \frac{1}{2}\left(\mathbf{F}(\boldsymbol{\sigma}_i^n, \mathbf{W}_i^n) + \mathbf{F}(\boldsymbol{\sigma}_{i+1}^n, \mathbf{W}_{i+1}^n)\right) - \frac{1}{2}\left|\widetilde{\mathcal{A}}_{i+1/2}\right|\cdot(\mathbf{W}_{i+1}^n - \mathbf{W}_i^n), \tag{14}$$

where Δt is the time step, $\Delta x = x_{i+1} - x_i$, $i = 1, \ldots, M$ is the size of the cells, $\mathbf{W}_i^n$ is the approximation of $\mathbf{W}(x_i, n\Delta t)$, given by the numerical scheme, $\widetilde{\mathcal{A}}_{i+1/2} = \widetilde{\mathcal{A}}(\widetilde{\mathbf{W}}_{i+1/2}^n)$, with $\widetilde{\mathbf{W}}_{i+1/2}^n = \frac{\mathbf{W}_i^n + \mathbf{W}_{i+1}^n}{2}$, being

$$\mathcal{A}(\boldsymbol{\sigma}, \mathbf{W}) = \begin{bmatrix} J(\sigma_1, W_1) & -B_1(W_1) \\ -B_2(W_2) & J(\sigma_2, W_2) \end{bmatrix}, \; J(\sigma_j, W_j) = \begin{bmatrix} 0 & 1 \\ -\dfrac{Q_j^2}{A_j^2} + \dfrac{g}{\sigma_j}A_j & 2\dfrac{Q_j}{A_j} \end{bmatrix},$$

$$\widetilde{\mathbf{B}}_{i+1/2} = \begin{bmatrix} 0 & B_1(\widetilde{\mathbf{W}}_{i+1/2}^n) \\ B_2(\widetilde{\mathbf{W}}_{i+1/2}^n) & 0 \end{bmatrix},$$

$$\widetilde{\bar{\mathbf{S}}}_{i+1/2} = \bar{\mathbf{S}}(x_{i+1/2}, \widetilde{\mathbf{W}}^n_{i+1/2}), \quad x_{i+1/2} = \frac{x_i + x_{i+1}}{2},$$

$$\mathbf{P}^{\pm}_{i+1/2} = \mathbf{K}_{i+1/2} \left(\mathbf{Id} \pm \mathrm{sgn}(\mathbf{\Lambda}_{i+1/2})\right) \mathbf{K}^{-1}_{i+1/2}, \tag{15}$$

where

$$\mathrm{sgn}(\mathbf{\Lambda}_{i+1/2}) = \begin{bmatrix} \mathrm{sgn}(\lambda_{i+1/2,1}) & & 0 \\ & \ddots & \\ 0 & & \mathrm{sgn}(\lambda_{i+1/2,4}) \end{bmatrix},$$

being $\lambda_{i+1/2,l}$, $l = 1, \ldots, 4$ the eigenvalues of $\widetilde{\mathcal{A}}_{i+1/2}$ and $\mathbf{K}_{i+1/2}$ the matrix whose columns are the eigenvectors corresponding to these eigenvalues. Source terms due to channel geometry are treated as in [3], [24].

Finally, $\widetilde{\mathbf{C}}_{i+1/2} = \begin{bmatrix} 0 \\ \widetilde{C}_{i+1/2,1} \\ 0 \\ \widetilde{C}_{i+1/2,2} \end{bmatrix}$ where

$$\widetilde{C}_{i+1/2,j} = \frac{g}{2}\left(\frac{A^2_{i+1,j}}{\sigma_{i+1,j}} - \frac{A^2_{i,j}}{\sigma_{i,j}}\right) - g\frac{\widetilde{A}_{i+1/2,j}}{\widetilde{\sigma}_{i+1/2,j}}(A_{i+1,j} - A_{i,j}),\ j = 1, 2, \tag{16}$$

with

$$\widetilde{A}_{i+1/2,j} = \frac{A_{i+1,j} + A_{i,j}}{2}, \widetilde{\sigma}_{i+1/2,j} = \frac{\sigma_{i+1,j} + \sigma_{i,j}}{2},\ j = 1, 2.$$

Remark 1 Note that the term $\mathbf{V}(\boldsymbol{\sigma}, \mathbf{W})$ does not appear explicitly in the numerical scheme. However, new terms ($\widetilde{\mathbf{C}}_{i\pm1/2}$) appear as consequence of the treatment of the spatial dependence of fluxes. The expression (16) is derived by imposing the numerical scheme to solve exactly the trivial steady state solution ($Q_1 = Q_2 = 0$). The same expression could be derived if the property of "conservation across discontinuities" is imposed (see [21]). See [6] for further details. ■

In order to prevent the numerical viscosity of the Q-schemes from vanishing when any of the eigenvalues of the matrices $|\widetilde{\mathcal{A}}_{i+1/2}|$ are zero, we apply Harten regularisation, [11]. In the deduction of the schemes CFL-like requirements have to be imposed (see [17]). In practice, we propose the following condition:

$$\frac{\Delta x}{\Delta t} \leq \gamma\ \max\{|\lambda_{l,i}|\,,\ |\ 1 \leq l \leq 4,\ 1 \leq i \leq M\},$$

where $0 < \gamma \leq 1$.

Finally, another numerical difficulties could appear in oceanographical applications:

- Kelvin-Helmholtz instabilities: These instabilities appear when the internal eigenvalues become complex. In this case the matrix $|\widetilde{\mathcal{A}}_{i+1/2}|$ in (14) has been redefined such that, the resulting numerical scheme guarantee the mass conservation (see [6] for more details).

- Treatment of cases when the thickness of a layer vanishes: These situations take place in lock-exchange computations or when the deeper Mediterranean waters are upwelled to surface. The extension of the techniques developed for the treatment of wet-dry situations for a single layer has been made (see [6] for more details).

4. Numerical results

4.1. Two-layer exchange flow through a contraction with local rectangular cross-sections

In this section the numerical results obtained by the finite volume model are compared with the approximate analytical solutions found by [1] and [2] (A&F hereafter) for steady flows through contractions. We have computed the transient from two of the stationary solutions given by A&F that are characterised by a constant value representing the difference of energy between the two layers of fluid. A periodic barotropic forcing to the two layer exchange flow through the contraction, as in [12], also has been imposed, obtaining periodical solutions.

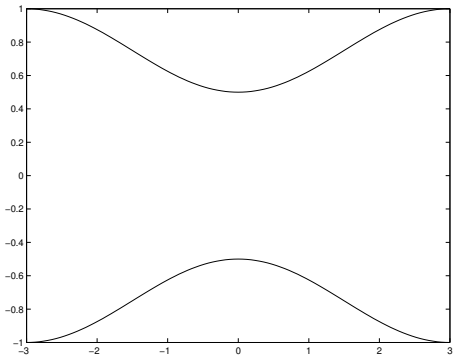

Figure 1. Sketch showing contraction plan view.

The strait geometry considered is sketched in Figure 1, that represents a symmetric contraction with no depth variations and with the origin located at the narrows,

$$\sigma(x) = 2 - \exp(-x^2),\ x \in [-3,3]; \quad b(x) = 0,\ x \in [-3,3].$$

The time dependent solutions that are obtained by the model change quantitatively, but not qualitatively, as the strait geometry is modified as is to be expected from *Armi and Farmer* hydraulic theory. *Armi and Farmer* model is based on the Bernoulli equations under the assumption of rigid lid. They parametrise the flows in terms of the internal Froude numbers for each layer, $F_i = u_i/\sqrt{(g'h_i)}$, and possible solutions to the steady two-layer exchange problem are shown as curves in the Froude-number plane (F_1^2, F_2^2). This parametrisation is done by the deduction of a dimensionless Bernoulli equation expressed in terms of F_1^2 and F_2^2:

$$\Delta H' = \frac{F_2^{-\frac{2}{3}}(1+\frac{1}{2}F_2^2) - \frac{1}{2}q_r^{\frac{2}{3}}F_1^{-\frac{2}{3}}F_1^2}{q_r^{\frac{2}{3}}F_1^{-\frac{2}{3}} + F_2^{-\frac{2}{3}}} \tag{17}$$

where $q_r = q_1/q_2$ is the ratio of flow rates at each layer. The term $\Delta H'$ is the dimensionless energy difference between the two layers. In the absence of friction, mixing or any other losses of energy, this quantity is conserved. Therefore, the curves verifying (17) with constant $\Delta H'$ represent the solutions of the model (where dissipative processes are not considered). These solutions haven been plotted in detail by [1], here, in Figure 2, we show an example for $q_r = 1$ and $q_r = 0.5$, where only physically feasible solutions are drawn.

To obtain the details of the solution corresponding to one of these curves, these authors make use of the Froude-number continuity equation:

$$q_r^{\frac{2}{3}}F_1^{-\frac{2}{3}} + F_2^{-\frac{2}{3}} = \left(\frac{q_2'}{\sigma'}\right)^{-\frac{2}{3}}. \tag{18}$$

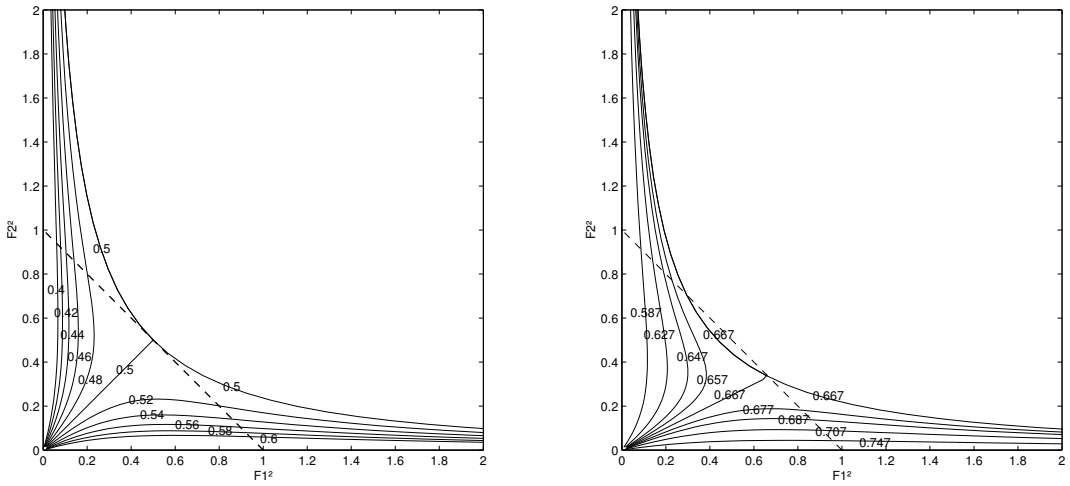

(a) $q_r = 1$. (b) $q_r = 0.5$.

Figure 2. Solutions to the Bernoulli equations in the Froude-number plane for $q_r = 1$ and $q_r = 0.5$. Each solution curve is labelled with its non-dimensional energy difference between the two layers.

Intersections between (17) and (18) serve to obtain the values of $\frac{q_2'}{\sigma'}$ for every (F_1^2, F_2^2)-couple. The prime variables representing the non-dimensional quantities. Besides, when we are located at the narrows the critical condition, $G^2 = F_1^2 + F_2^2 = 1$, is achieved and $\sigma' = 1$. Observe that $G^2 = F_1^2 + F_2^2$ is an approximation of the *composite Froude number*

$$G^2 = F_1^2 + F_2^2 - (1 - r)F_1^2 F_2^2 = 1$$

for $r \cong 1$. This allows us to determine q_2' for the corresponding steady solution and consequently q_1', as q_r is fixed. Then, the dimensionless layer thickness are recovered from the expression:

$$h_i' = \left(\frac{q_i'}{\sigma'}\right)^{\frac{2}{3}} F_i^{-\frac{2}{3}}. \tag{19}$$

In Figure 2(a) the (dashed) line $F_1^2 + F_2^2 = 1$ represents critical points and separates supercritical from subcritical flows. The $\Delta H' = 0.5$ curve represents the maximal two-layer exchange solution (in the sense that is the solution -physically feasible- permitting a maximal exchange flow). This curve separates stable (that are the sole solutions shown in Figure 2) from instable flows. It can be observed that the maximal solution is the sole solution for which the flow is supercritical everywhere along the contraction. The rest of solutions are called submaximal and are subcritical to one side of the control, that is located at the narrows, and supercritical to the other side. In Figure 2(b) for $q_r = 0.5$, it can be observed that the maximal solution (for $\Delta H' = 0.667$) presents two control points, one located at the narrows and the second one, the so-called *"virtual" control*, located to its right (for the flow configuration chosen here with the upper layer flowing from left to right and the lower layer moving in opposite direction, being the denser basin to the right and the lighter one to the left). The zone located between the two controls being called *"control region"*.

The first experiment performed consisted in taking as initial conditions A&F's steady solution for $q_r = 1$ and $\Delta H = 0.54$. As boundary conditions the input flow at the right end of the contraction for the lower layer and the input flow at the left side for the upper layer were imposed, being $q_1(-3, t) = q_2(3, t)$ for all time t, and a density ratio $r = 0.98$ was chosen. Then, the flux is increased up to reach the value corresponding to the $\Delta H = 0.52$ A&F stationary solution at $t = 2000$ s. Once the flux remains unchanged, the steady solution is rapidly reached. Figure 3(a) shows the evolution of the interface along the channel from $\Delta H = 0.54$ A&F solution, corresponding to the $t = 0$ (solid) line, to the $\Delta H = 0.52$ solution. The

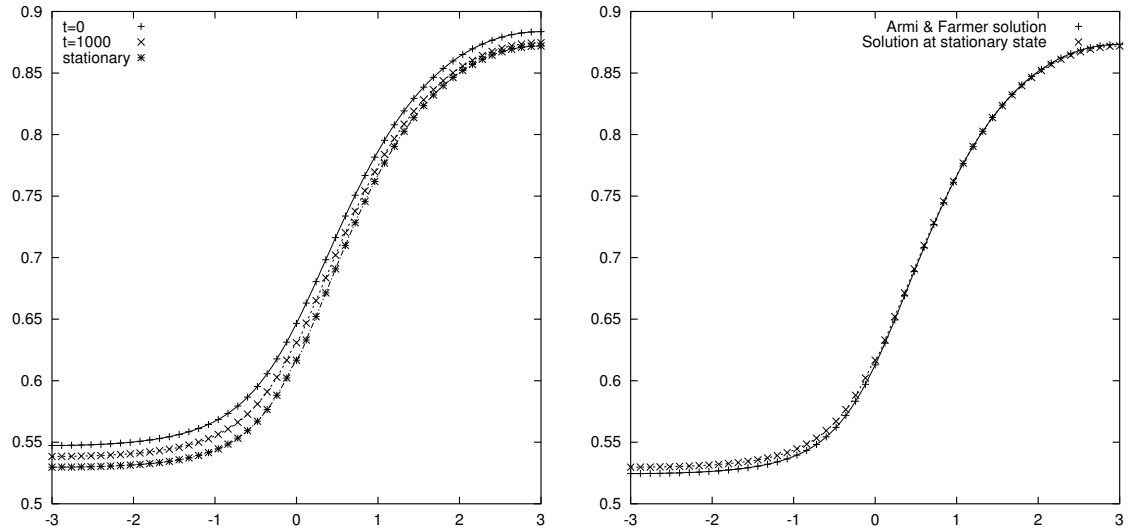

(a) Interface at t=0, t=1000 and the stationary state.

(b) Stationary state and A&F solution.

Figure 3. Transition from $\Delta H = 0.54$ to $\Delta H = 0.52$ energy level stationary states and comparison with the solution found by A&F for $\Delta H = 0.52$.

two constant energy solutions considered represent submaximal flows, whose composite Froude numbers, $G^2 = F_1^2 + F_2^2$, along the channel are qualitatively as in Figure 5(a), reaching the value $G = 1$ at the narrows. The eigenvalues associated to these solutions are also analogous to those in Figure 5(b).

Figure 3(b) shows the final stationary state reached in the experiment performed here compared with the stationary approximate solution obtained by A&F and corresponding to the constant $\Delta H = 0.52$ energy level. Note that the solutions given by A&F are asymptotic approximations when $r \to 0$ and that they are deduced under the assumption of rigid lid, whilst the model used here is a free surface model with two layers of different densities.

4.1.1. Periodic barotropic forcing

In [12] a model is presented for the study of time-dependent two-layer hydraulic flows through straits. The model is used to simulate flows forced by a periodic barotropic (tidal) flow. This author must add some dissipation to his model to control the appearance of unphysical instabilities. In the experiment presented here we try to reproduce the experiment presented in [12] for a contraction.

As initial conditions we consider the steady state corresponding to $\Delta H' = 0.54$. At the boundaries, only q_1 and q_2 are imposed on the left border. The barotropic transport considered is periodic with zero time mean and given by $q_b(t) = q_{b_0} \sin(2\pi t/T)$, where $q_{b_0} = 9 \cdot 10^{-3}$ is the barotropic transport amplitude and $T = 800$ is the period. For these parameters the forcing is relatively weak and similar to that given for the experiment shown in Figure 4 of [12].

Figure 4(a) depicts the interface along the contraction at four points through the forcing period. The interface moves back-downwards and forth-upwards, with the barotropic flow but still similar in shape to the steady solutions. The periodic solution is obtained from the initial state without any prior adjustment period.

In Figure 4(b) we show the same four transient solutions in the Froude number space (F_1^2, F_2^2). The intersection between curves indicates that the four transients do not correspond to a succession of constant $\Delta H'$ steady solutions with $q_r = 1$, as proposes the quasi-steady theory. This approximation supposes time-dependent problems as a succession of steady states. Such hypothesis is supposed to be valid provided that

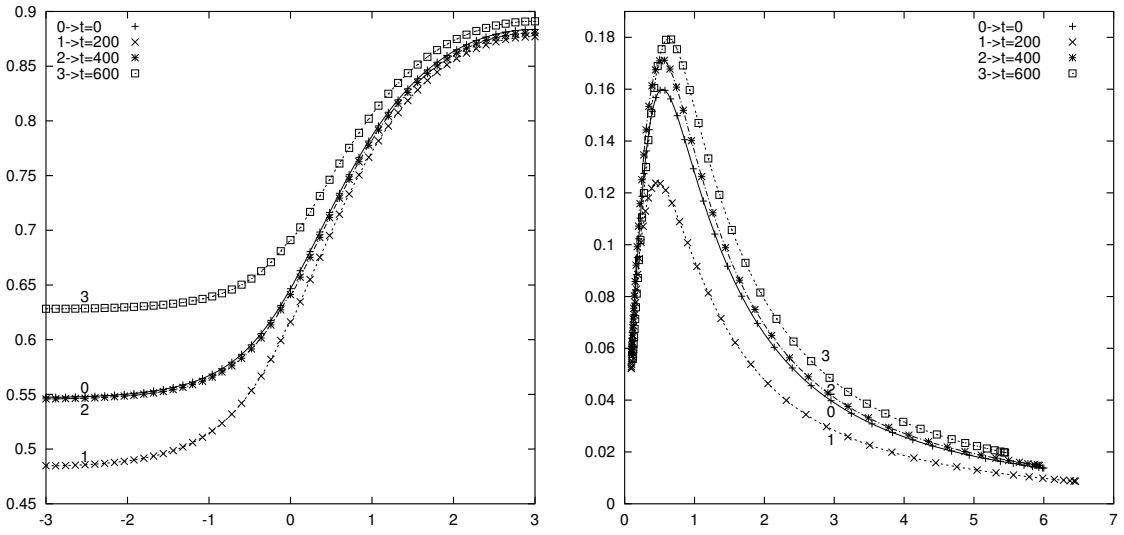

(a) Interface at four points through the forcing period.

(b) Transient solutions in the Froude number diagram (F_1^2, F_2^2).

Figure 4. Exchange flow forced by a periodic barotropic flow.

the tidal (periodic forcing) effect is slow relative to the time taken for interfacial adjustment (the time taken by long waves to propagate through the channel must be short compared with the tidal period). Although this may be the case in many natural straits, it seems that time dependence modifies the dynamics so that the steady model fails. We must remark that, in the time-dependent problem, the flow is not exactly constant along the channel for time fixed.

Figure 5(a) shows the composite Froude number G^2 along the channel at time $t = 400$ for the experiment with barotropic forcing. This Figure shows that the flow is subcritical to the left of the narrows, critical at the narrows and supercritical to the right, being the exchange submaximal. This situation remains so along all the forcing period. Figure 5(b) shows the four eigenvalues for the transient solution with barotropic forcing at $t = 400$. The internal eigenvalues are represented by the lines closer to the x-axis. It can be observed how one of these eigenvalues becomes zero at the narrows, being two eigenvalues positives and two negatives in the subcritical region, and three positive and one negative in the supercritical region.

4.1.2. Maximal exchange solution

In order to reproduce a maximal exchange solution, we solve the classical *lock exchange problem*. This problem consists in taking as initial state the two fluids separated by a vertical "artificial barrier" in this case located at the narrowest channel section (see Figure 6(a)) . This barrier is dropped out at time $t = 0$ and fluids are let evolve until a stationary state is reached (see Figure 6(b)). In the numerical experiment presented here, the same channel geometry as in former section is considered. As boundary conditions only the ratio between fluxes is imposed and it is set to 1, i.e., $Q_1 = -Q_2$ at each channel end. The ratio between densities $r = \rho_1/\rho_2$ has been taken equal to 0.98. Figure 6(b) shows the final steady state reached and compares it against the corresponding maximal A&F solution. The exchange flux predicted by the model is $Q_1 = -Q_2 = 1.111\,10^{-1}$ m^3/s while F&A model gives $Q_1 = -Q_2 = 1.107\,10^{-1}$ m^3/s (transforming adimensional quantities provided by F&A into dimensional variables).

Figure 7(a) shows the internal eigenvalues along the channel for the computed stationary solution. As formerly observed, the maximal solution is, in this case, supercritical everywhere (only a small control region appears located at x=0 as consequence of Harten's regularisation). The representation of the maximal

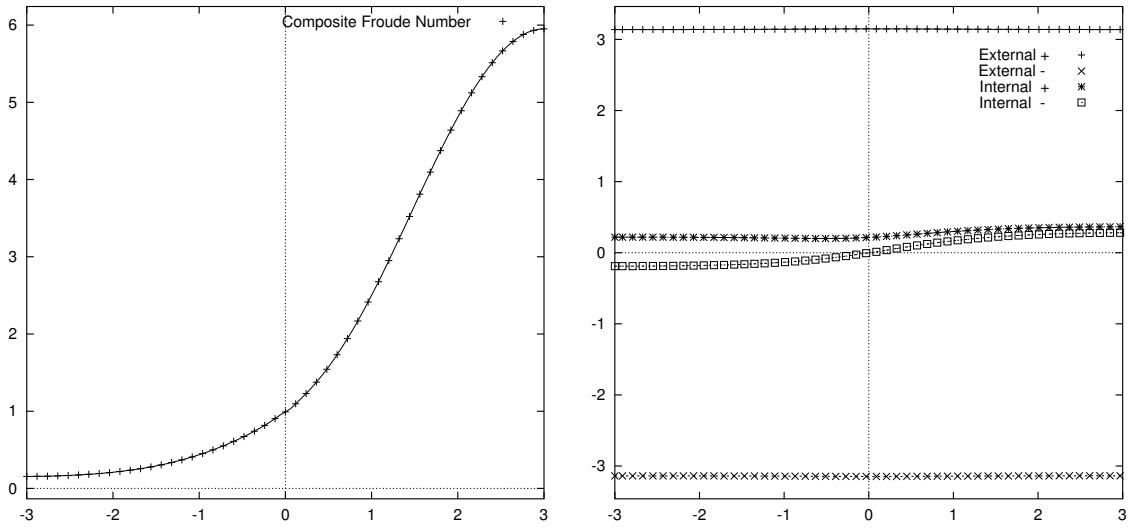

(a) Composite Froude numbers along the channel.

(b) Eigenvalues along the channel.

Figure 5. Exchange flow forced by a periodic barotropic flow at t=400.

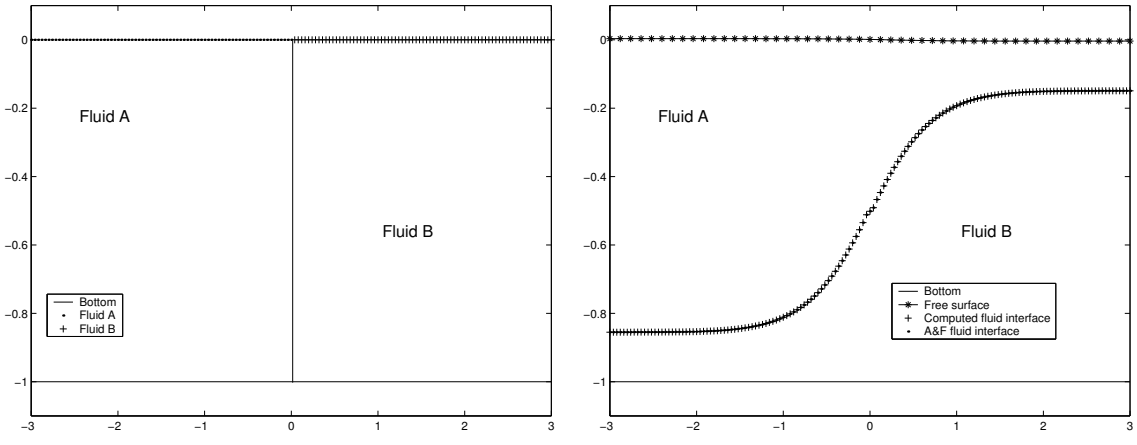

(a) Initial condition

(b) Stationary state and comparison with A&F solution

Figure 6. Maximal exchange flow through a rectangular channel with a contraction. Initial condition and comparison with A&F stationary solution

solution in the Froude-number plane is shown in Figure 7(b). As this maximal solution is also characterised as been the curve that separates stable from instable flows, this implies that the two internal eigenvalues must coincide along the channel (see Figure 7(a)).

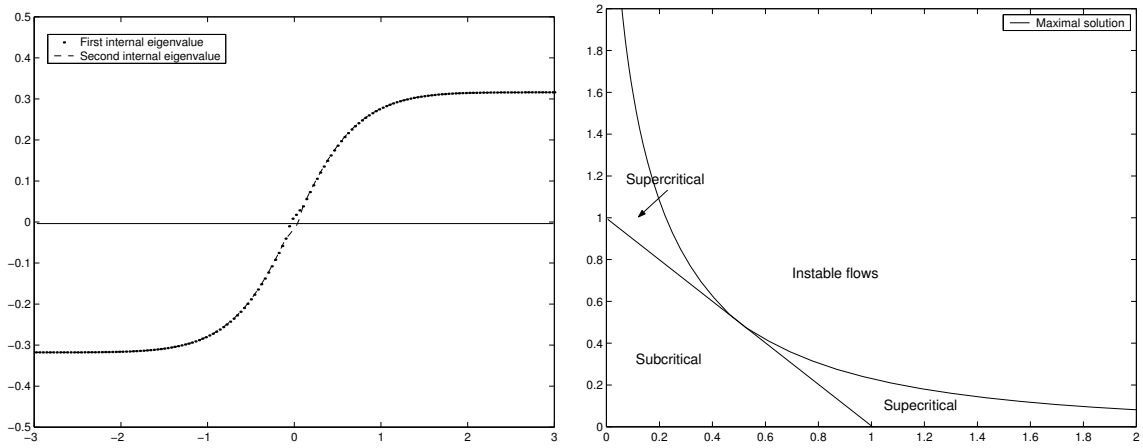

(a) Internal eigenvalues (b) Maximal solution in the Froude-number plane

Figure 7. Internal eigenvalues of the maximal exchange flow for $q_r = 1.0$ and its representation in the Froude-number plane

4.2. Two-layer exchange flow through a combination of offset sill and narrows with local rectangular cross-sections

In this section we perform a comparison between the numerical results obtained by using the numerical scheme proposed in section 3 for a two-layer exchange flow through a channel with a combination of offset sill and narrows. As in the previous section three different simulations have been performed. In the first one, an approximate stationary solution is computed and compared with the approximate "generalized A&F solutions" (GA&F hereafter) deduced in [15] for more general geometry channels. The second experiment consists in imposing a periodic barotropic forcing to the two layer exchange through this new geometry analogously as in [12], where periodic solutions are obtained. Finally a maximal exchange solution is computed.

In all cases, the same channel geometry, given by the functions (see Figure (8)).

$$b(x) = \frac{1}{\cosh^2(3.75x)},\ x \in [-1,2],$$

$$\sigma(x) = 0.5 + 1.5(1 - e^{-a^2(x-1)^2}),\ x \in [-1,2],\ a = \begin{cases} 0.637 \text{ if } x \leq 1 \\ \\ 1.273 \text{ if } x > 1. \end{cases}$$

has been considered. These functions determine a channel with a sill placed at $x = 0$ and a contraction located at $x = 1$.

4.2.1. Generalized Armi and Farmer steady solutions

As we have presented in the previous sections, Armi and Farmer obtained approximate stationary solutions of two-layer exchange flows through contractions (in [1] and [2]) and over sills (in [1] and [8]). In [8], they also study the case of a combination of sill and contraction, but without determining the details of

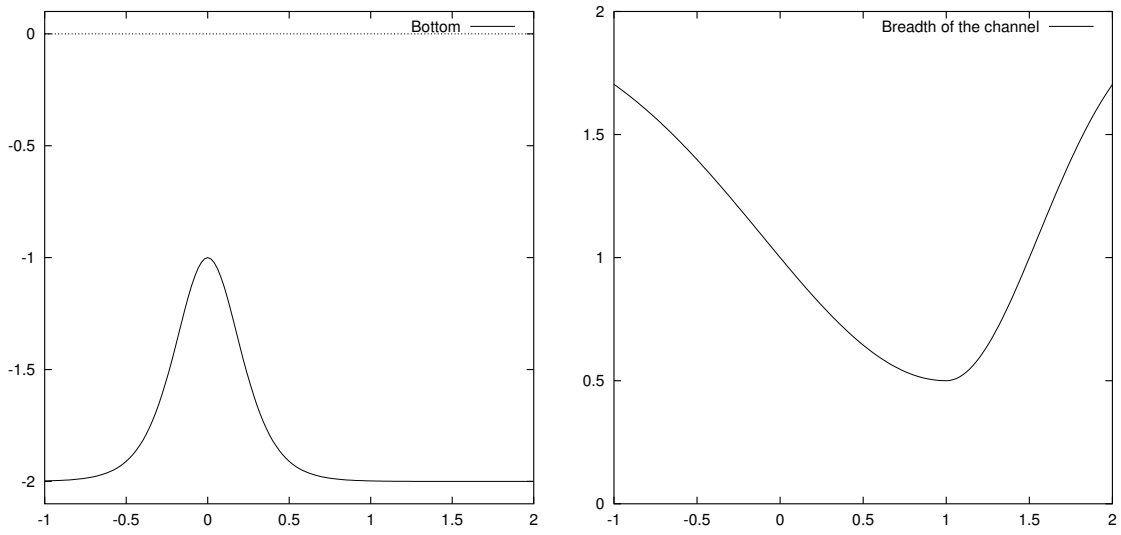

(a) Depth of the channel. (b) Breadth of the channel.

Figure 8. Channel geometry: depth and breadth.

the solutions as they did for single sills and contractions. More recently, Macías in [15] has extended their works to general geometries (among them combinations of sills and contractions). The price to be paid is that is necessary to know the geometry defining the channel. As in Armi and Farmer, the model is based on the Bernoulli equations under the assumption of rigid lid and the flow is parametrized in terms of the internal Froude numbers for each layer F_i, being the steady state solutions determined as curves in the Froude-number plane (F_1^2, F_2^2).

The experiment performed consists in taking

$$\begin{cases} h_1(0,x) = 1.3 - b(x), \\ h_2(0,x) = 0.7, \\ q_1(0,x) = q_2(0,x) = 0, \end{cases}$$

as initial conditions and

$$\begin{cases} q_1(t,2) = q_1^R, \\ q_2(t,-1) = q_2^L,\ q_2(t,2) = q_2^R, \end{cases}$$

as boundary conditions, where q_1^R, q_2^L and q_2^R are the values corresponding to a given stationary GA&F solution at channel boundaries.

Figures (9(a)) and (9(b)) show respectively the initial and the final stationary states reached in the experiment performed. In Figure (9(b)), the final state is compared with the corresponding GA&F approximate solution.

4.2.2. Periodic barotropic forcing

As in the previous section, we present here a numerical experiment similar to one of the experiments presented in [12]. As initial condition the steady state solution obtained in the experiment presented in

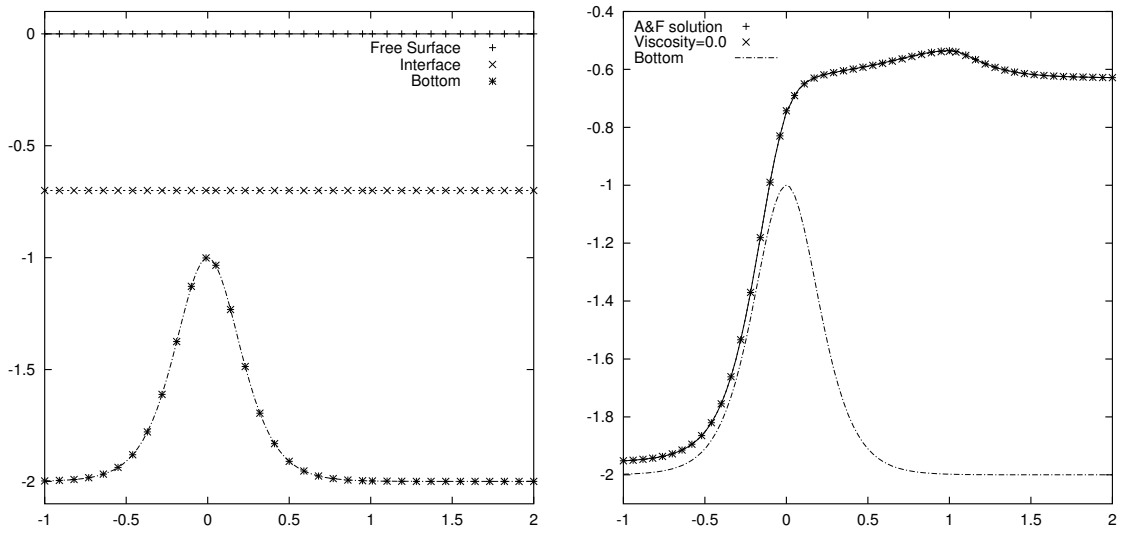

(a) Initial condition.

(b) Stationary solution and comparison with GA&F solution.

Figure 9. Stationary solution and generalized A&F solution.

the previous section has been taken. At the boundaries, q_1 and q_2 are imposed only on the right end of the channel. The barotropic transport considered is periodic with zero time mean and given by $q_b(t) = q_{b_0} \sin(2\pi t/T)$, where $q_{b_0} = 5 \cdot 10^{-3}$ is the barotropic transport amplitude and $T = 800$ is the period.

Figure (10) depicts the interface along the channel at four different times through the forcing period. The behaviour of the obtained solution is similar to that described in Figure 10 of [12]: the interface moves back-downwards and forth-upwards, with the barotropic flow but still similar in shape to the steady solution computed in the previous experiment. The periodic solution is obtained from the initial state without any prior adjustment period.

4.2.3. Maximal exchange solution

As in the previous example, in order to reproduce a maximal exchange solution, we solve a *lock exchange problem* now in this channel. In this case, the artificial barrier separating the two fluids is located at the top of the sill (see Figure 11(a)). The barrier is dropped out at time $t = 0$ and fluids are let evolve until a stationary state is reached (see Figure 11(b)).

As in the previous example, as boundary conditions only the ratio between fluxes is imposed and it is set to 1. The ratio between densities $r = \rho_1/\rho_2$ has also been taken equal to 0.98. Figure 11(b) shows the final steady state reached. The exchange flux predicted by the model is $Q_1 = -Q_2 = 6.126\,10^{-2}$ m^3/s.

Figure 12 shows the internal eigenvalues along the channel for the computed stationary solution. Three different regions separated by two control points (null internal eigenvalues), located at the points of minimal depth and breadth, respectively, can be observed. In the middle one, the flow is subcritical and it is named "control region". In the other two located at the two ends of the channel, the flow is supercritical.

4.3. Strait of Gibraltar

Now we present some numerical results obtained for the application of the model to a channel playing the role of the Strait of Gibraltar. To obtain a suitable one-dimensional representation of this narrows an "equivalent" symmetric channel that preserves cross-section areas is first constructed. This is done as follows: From realistic bathymetric and coast line data, an axis defining the Strait orientation is settled.

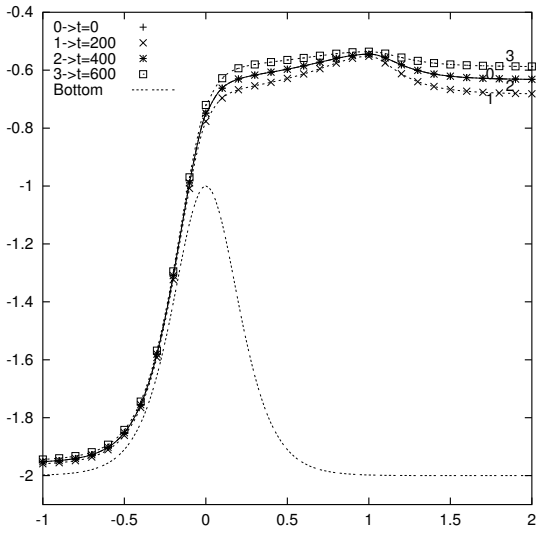

Figure 10. Exchange flow forced by a periodic barotropic flow.

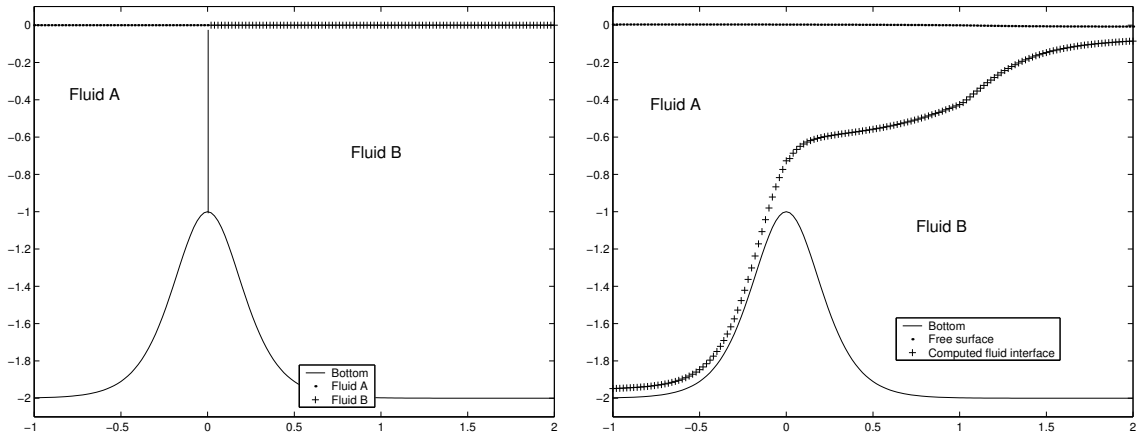

(a) Initial condition (b) Stationary state

Figure 11. Maximal exchange flow through a rectangular channel with a contraction. Initial condition and comparison with A&F stationary solution

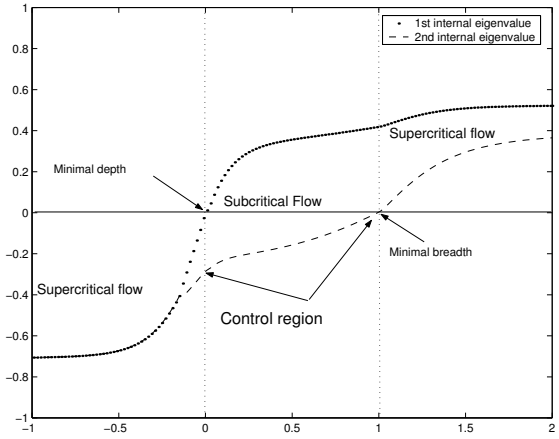

Figure 12. Internal eigenvalues along the channel.

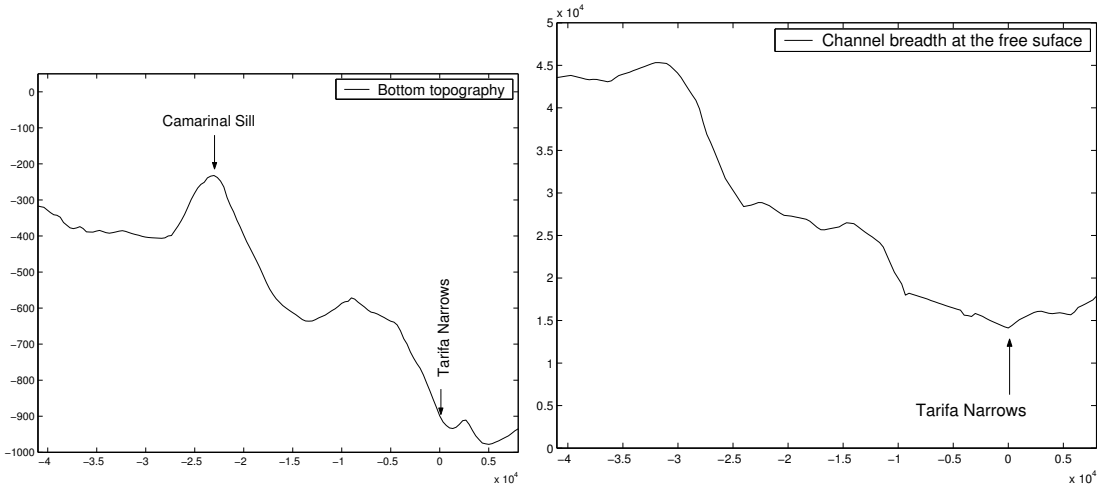

(a) Bottom topography (b) Channel Breadth

Figure 13. Geometry of the channel (Strait of Gibraltar)

Along this axis we consider $M = 150$ transversal cross-sections, S_i, $i = 1, \ldots, M$, whose areas are numerically computed. The bottom topography, at each of these sections, is taken as the maximal depth, b_i, found in the bathymetric data. Finally, channel breadth is defined as a continuous piecewise linear function so that the cross-section areas are preserved. We would like to remark that cross-sections are defined by polygonal lines, that means that we are working with more general cross-sections that rectangular (as in the first numerical example presented here or as in *Armi & Farmer* model) or more general than simply triangular cross-sections. In Figure 13(a) the bottom topography obtained with the bathymetric data used

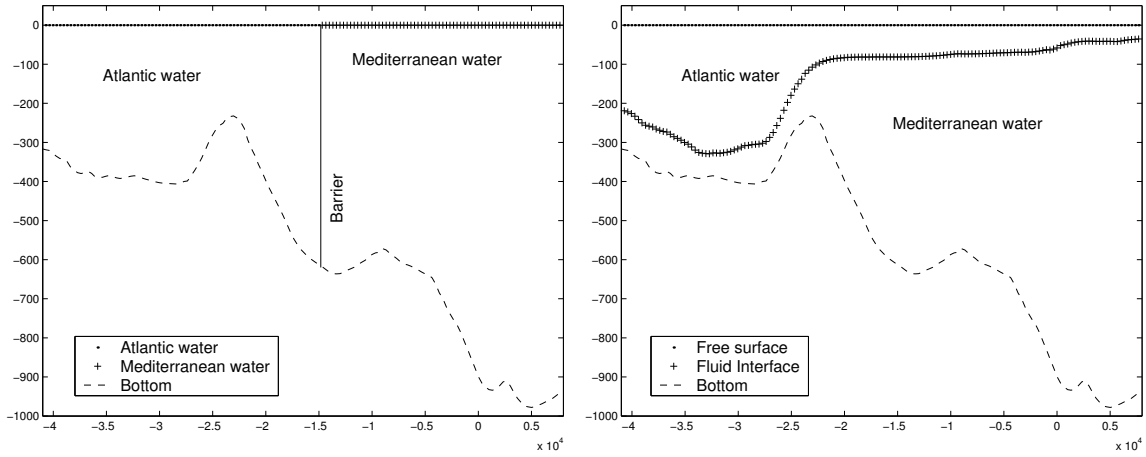

(a) Initial conditions (b) Free surface and interface

Figure 14. Interface and free surface of a maximal exchange flow through the Strait of Gibraltar

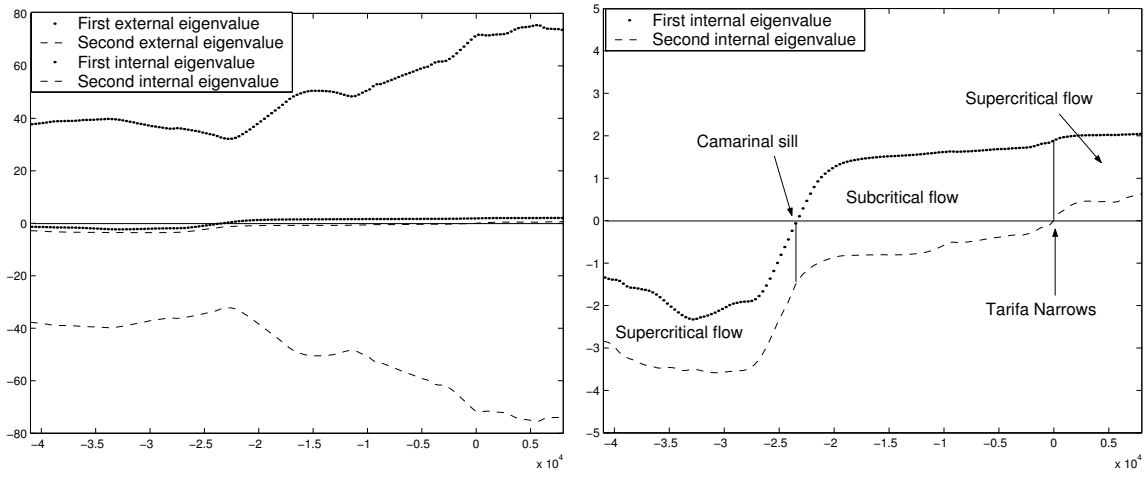

(a) Internal and external eigenvalues (b) Internal eigenvalues

Figure 15. Eigenvalues along the Strait for the computed maximal solution

is shown. The two key locations corresponding to the shallowest and narrowest sections along the Strait of Gibraltar are also marked in the figure. They correspond to Camarinal Sill and Tarifa Narrows, respectively. Figure 13(b) depicts the breadth at water surface of the equivalent symmetric channel.

4.3.1. Maximal solution

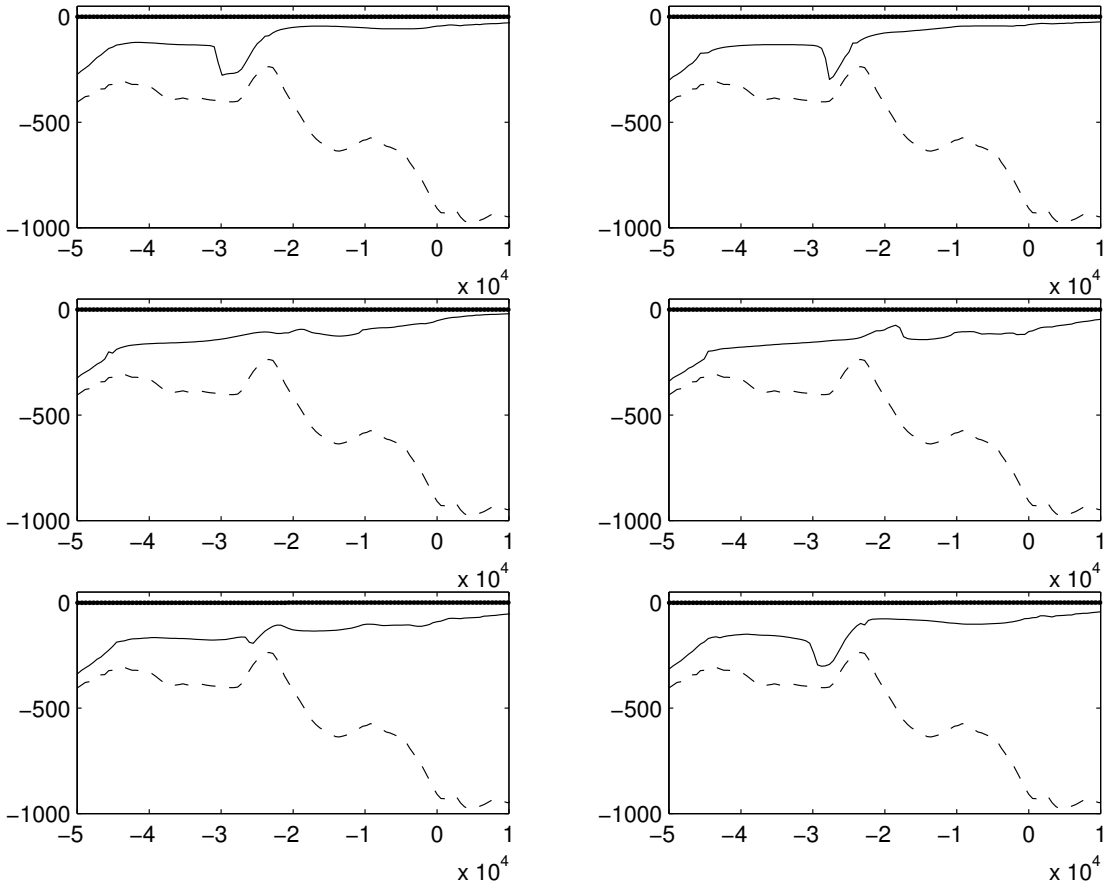

Figure 16. Evolution of the interface and free surface during a tidal forcing period.

Figure 14(a) shows the bottom together with the initial condition where the Atlantic waters on the left are separated by an artificial barrier from the Mediterranean denser waters on the right. The ratio of densities is taken equals to 0.99805.

Figure 14(b) depicts the interface and free surface of the stationary state reached when, as boundary condition, we impose the ratio between fluxes at both ends of the Strait. This ratio is taken as unity. The simulated exchange flow is $Q_1 = -Q_2 = 0.855$ Sv, magnitude that agrees with the experimental data (see, for example, [4])

Figure 15(a) shows all the four eigenvalues for the stationary maximal solution reached in the numerical experiment presented here. In Figure 15(b) a zoom on the two internal eigenvalues is shown. It can be observed the appearance of two control points (null internal eigenvalues) essentially located at Camarinal Sill (minimal depth) and at Tarifa Narrows (minimal breadth). These two controls separate a region where the flow is subcritical called “control region” from the supercritical flow found at the two ends of the channel.

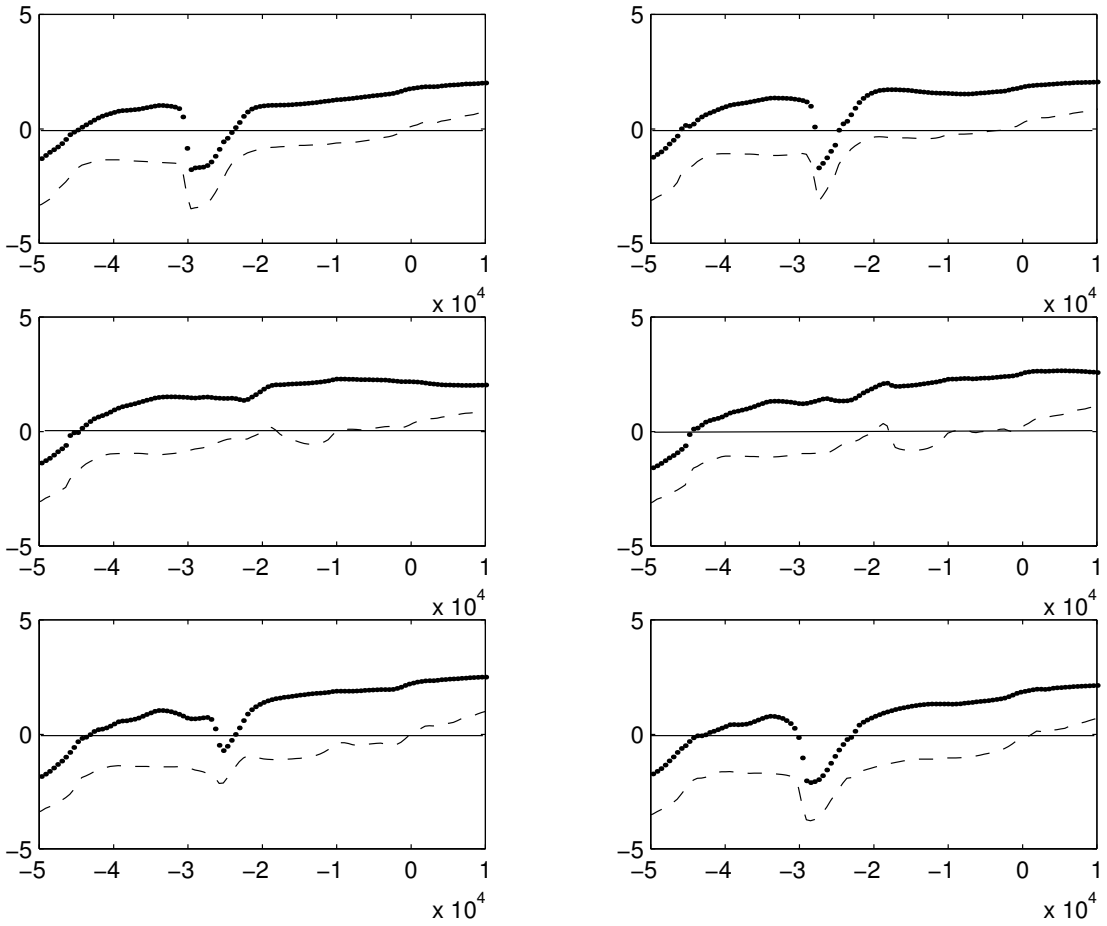

Figure 17. Evolution of the internal eigenvalues during a tidal forcing period.

4.3.2. Tidal forcing

Oscillations of the surface level due to tides are more important in the Atlantic and produce strong tidal currents. These tidally induced currents interact with the prominent underwater bottom features, in particular with the Camarinal Sill, generating strong internal tides and eastward propagating internal waves. The surface currents associated with internal waves disturbances cause distinctive surface roughness patterns that has been detected by radars and observed in aerial photographs and satellite images.

The purpose of the experiment presented here was to simulate the evolution of the interface through a tidal period in the Strait of Gibraltar and to study the eventual generation and propagation of internal waves. The model was run for 10 semidiurnal tidal cycles, which has a period of $T = 12.4$ hours, to achieve a stable time-periodic solution, using as initial condition the previous maximal flux exchange solution. After establishing this periodic solution, model integration was continued for a 7-day period. Tidal forcing was imposed by means of the boundary conditions by giving the elevation of the free surface at the two ends of the channel by the time-dependent functions

$$\phi_L(t) = \sum_{n=1}^{N} A_n^L cos(\theta_n^L t - \sigma_n^L), \qquad \phi_R(t) = \sum_{n=1}^{N} A_n^R cos(\theta_n^R t - \sigma_n^R),$$

where A_n^L and σ_n^L (A_n^R and $\sigma^R L_n$ respectively) are the prescribed surface elevation amplitude and phase of the n-th tidal constituent at the left (right respectively) end of the channel; θ_n^L (θ_n^R respectively) is its frequency and N is the number of tidal constituents. In this simulation the M_2, S_2, K_1 and O_1 surface tidal elevation are used to set the tidal forcing, being the values for the amplitudes and phases taken from [14]. These values are given at some coast points. Here we use the mean value of the values at the two locations determining the corresponding limiting section.

In Figure 16 the free surface (dotted) and the interface (continuous line) is depicted for six different phases of the tidal cycle. The evolution of the internal eigenvalues for the same tidal phases is shown in Figure 17. During strong westward flow, interfacial depressions are presented west of Camarinal Sill (Figure 16a). In this case the barotropic forcing is the same direction as the steady outflow at depth and the interface upstream of the Camarinal Sill is pushed toward shallower depths. Nearly always two control regions with subcritical flow are found, one bounded by Spartel Sill and some point west of Camarinal Sill, the second between Camarinal Sill and Tarifa Narrows. Bounding these two control regions the flow is supercritical (see Figure 17). Observe how the tidal forcing change the location of the critical and subcritical regions from the base state (the maximal exchange solution) generating a new and permanent critical point at Spartel Sill not found in the maximal solution (compare Figure 17 with 15(b)). When the westward tidal flow slackens (see Figure 16c) some interfacial waves are released from Camarinal Sill and propagate eastward. With the reversal of the tidal flow an internal bore is produced that is advected eastward (Figure 16d). During this phase the flow is basically subcritical everywhere from Spartel Sill to Tarifa Narrows (see Figures 17c and 17d). The asymmetry in the strength of internal hydraulic jumps at the Camarinal Sill during strong westward and eastward tidal flow, which is due to the mean flow in the lower layer, leads to an east-west asymmetry in the internal wave field; westward propagating internal waves are much weaker than eastward propagating ones.

5. Final remarks

In this work the computation of maximal two-layer exchange solutions through channels with irregular geometry is undertaken. We have been able to properly reproduce this type of solutions by solving the classical lock exchange problem without adding any artificial viscosity in the mathematical model as it is common practice when discretizing by finite differences. Model performance has been assessed by comparing the numerical results against the analytical approximate solutions provided by *Armi & Farmer*. Finally, the model is used to simulate the maximal exchange flow through the Strait of Gibraltar by considering a suitable one-dimensional representation of its realistic geometry. The numerical fluxes obtained agree

with the observational data currently available. The model is also used to perform tidal simulations. Future lines of research focused on the validation of such numerical results for tidally induce flows in the Strait of Gibraltar. Currently we are working on a two-dimensional two-layer model based on the same numerical techniques than the ones used in the model presented here. Similar studies to the ones developed for the one-dimensional model are also foreseeable.

Acknowledgement. his research has been partially supported by the C.I.C.Y.T. (project REN2000-1168-C02-01). Thanks are given to Alfredo Izquierdo for providing us the bathymetric data.

References

[1] Armi, L. (1986). The hydraulics of two flowing layers with different densities, *J. Fluid Mech.*, **163**, 27–58.

[2] Armi, L. and D. Farmer, D. (1986). Maximal two-layer exchange through a contraction with barotropic net flow, *J. Fluid Mech.*, **164**, 27–51.

[3] Bermúdez, A. and Vázquez, M.E. (1994). Upwind methods for hyperbolic conservation laws with source terms, *Computers and Fluids*, **23**(8), 1049–1071.

[4] Bryden, H., Candela, J. and Kinder, T. H. (1994). Exchange through the Strait of Gibraltar, *Prog. Oceanogr.*, **33**, 201–248.

[5] Castro, M. J., Macías, J. and Parés, C. (2001). A Q-Scheme for a class of systems of coupled conservation laws with source term. Application to a two-layer 1-D shallow water system, *Math. Model. and Numer. An.*, **35**(1), 107–127.

[6] Castro, M. J., Macías, J., Parés, C. and Vázquez-Cendón, M. E. (2002). On the numerical treatment of a two-layer model for flows through channels with irregular geometry. Applications. *In progress*.

[7] Cunge, J. A., Holly, F. M. and Verwy, A. (1980). *Practical Aspects of Computational River Hydraulics*. Massachusetts Pitman Pub. Inc. Massachusetts.

[8] Farmer, D. and Armi, L. (1986). Maximal two-layer exchange over a sill and through a combination of a sill and contraction with barotropic flow, *J. Fluid Mech.*, **164**, 53–76.

[9] Gill, A. E. (1982). *Atmosphere-Ocean Dynamics*, volume 30 of *Int. Geophys. Series*. Academic Press Inc.

[10] García-Navarro, P. and Vázquez-Cendón, M. E. (2000). On numerical treatment of the source terms in the shallow water equations, *Computers and Fluids*, **29**(8), 17–45.

[11] Harten, A. (1984). On a class of high resolution total-variation-stable finite-difference schemes, *SIAM J. Numer. Anal.*, **21**(1), 1–23.

[12] Helfrich, K. R. (1995). Time-dependent two-layer hydraulic exchange flows, *J. Phys. Oceanogr.*, **25**(3), 359–373.

[13] Kundu., P.K. (1990). *Fluid Mechanics*, Academic Press, Inc.

[14] García-Lafuente, J. M., Almazán, J. L., Castillejo, F., Khribeche, A. and Hakimi, A. (1990). Sea level in the Strait of Gibraltar: Tides, *Intern. Hydrogr. Rev.*, **LXVII**(1), 111–130.

[15] Macías, J. (2001). Approximate Armi and Farmer solutions for flows through arbitrary channels, *Internal Journal 0115, group on "Differential Equations, Numerical Analysis and Applications*, University of Málaga, Spain.

[16] Macías, J., Castro, M. J. and Parés, C. (2002). Armi and Farmer hydraulic theory as a method for two-layer 1D model validation, *Submitted*.

[17] Roe., P. L. (1981). Approximate Riemann solvers, parameter vectors and difference schemes, *J. Comput. Phys.*, **43**, 357–371.

[18] Roe, P. L. (1986). Upwinding differenced schemes for hyperbolic conservation laws with source terms. In Carasso, Raviart, and Serre, editors, *Proc. of the Conference on Hyperbolic Problems*, 41–51. Springer.

[19] Schijf, J.B. and Schonfeld, J.C. (1953). Theoretical considerations on the motion of salt and fresh water. In *Proc. of the Minn. Int. Hydraulics Conv.*, 321–333. Joint meeting IAHR and Hyd. Div. ASCE., Sept.

[20] Stoker. J. J. (1957). *Water Waves*. Interscience, New York.

[21] Toro, E. F. (1997). *Riemann Solvers and Numerical Methods for Fluid Dynamics. A Practical Introduction*. Springer.

[22] Toro, E. F. and Vázquez-Cendón, M. E. (2000). Model hyperbolic systems with source terms: exact and numerical solutions. *In Godunov Methods: Theory and Applications*. Kluwer Academic Plenum Publishers, 897–902.

[23] Vázquez-Cendón, M. E. (1994). *Estudio de Esquemas Descentrados para su Aplicación a las leyes de Conservación Hiperbólicas con Términos Fuente*. PhD thesis, Universidad de Santiago de Compostela.

[24] Vázquez-Cendón, M. E. (1999). Improved treatment of source terms in upwind schemes for the shallow water equations in channels with irregular geometry, *J. Comp. Physics*, **148**, 497– 526.

M. J. Castro, J. M. González-Vida, J. Macías, M. L. Muñoz, C. Parés
Dpto. de Análisis Matemático
Universidad de Málaga
29080-Málaga.
España

J. A. García-Rodríguez, E. Vázquez-Cendón
Dpto. de Matemática Aplicada
U. de Santiago de Compostela
15706-Santiago de Compostela
España